Politecnico di Milano

Dipartimento di Ingegneria Aerospaziale

Turbulent flow in a helically coiled pipe: an endoscopic PIV study

Sara Ceccon, Franco Auteri, Arturo Baron, Marco Belan,
Giuseppe Gibertini, Maurizio Quadrio

Scientific Report
DIA-SR 06-09

2006

.

Scientific Report DIA-SR 06-09

Published by
Politecnico di Milano, Dipartimento di Ingegneria Aerospaziale
Campus Bovisa
via La Masa 34
20156 Milano, Italy

Printed in Italy
December 2006

Contents

Introduction

The study of a turbulent flow in helically coiled pipe is important both for its engineering applications and its scientific interest. It is evident in many scientifi papers, among which for example the review article by Berger, Talbot and Yao [1], that many industrial processes require curved ducts to operate transport of physical quantities while satisfying space and geometric requirements: heat exchangers, chemical reactors, exhaust gas ducts of engines, evaporators, condensors, storage tanks, piping systems. Flow in curved pipe is also important in bioengineering applications (i.e. blood flow in the human arteria system).
The laminar flow in a coiled pipe has been studied in detail in the recent past, and today can be considered well explained (see e.g. [2–4]). The turbulent regime however, despite its pervasive interest, remains poorly understood to date, and numerical and experimental investigations are currently carried out to understand transition to turbulence [5, 6] as well as the fully-developed turbulent regime [7–9].
The flow through a helical coil differs from that through a straight pipe because of the secondary flows which arise from the imbalance between the centrifugal force (directed in the outward direction) and pressure force (directed inward) acting on a fluid element. These secondary flows consist of counter-rotating structures (see Figure 1), called Dean flows [1], which can influence heat and mass transfer. The curvature of the coil tends to dampen high-frequency turbulent fluctuations, so that a higher value of Reynolds number is necessary to establish a fully developed turbulent flow compared to the straight pipe [5]. Furthermore the point of maximum axial velocity, located in the center of the cross section for straight pipe, moves to the outward direction, as shown in [1].
Aim of this research project, partly financed by a PRIN 2004 grant, is to describe the turbulent flow in a helical pipe of circular cross-section, and in particular to study the secondary structures in turbulent conditions with an endoscopic Particle Image Velocimetry (PIV) technique (for a detailed

[1] Secondary flows in curved ducts are usually called "Dean vortices" by many authors (i.e. [5, 10–13]). However, Hüttl and Friedrich in [9] show that no significant pressure minima can be observed at the center of these structures, therefore the word *vortex* may be improper. For this reason in the present work the expression "Dean flows" will be used.

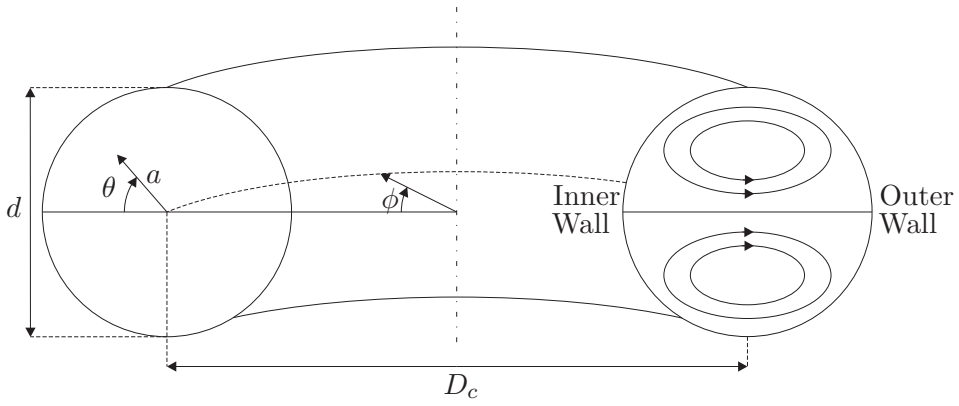

Figure 1: Sketch of the toroidal coordinate system, with indicatioin of the secondary flows.

handbook about PIV see [14]). In the available literature experimental studies are reported for the helical coil problem based on Laser–Doppler Velocimetry [5] or flow visualization [13]. The work documented here is, to our knowledge, the first attempt to use an intrusive technique. The whole experimental system (its configuration, required materials, instrumentations, etc) had to be studied and realized from scratch. Therefore the project started off with feasibility studies, preliminary evaluations, choice and verification of the instrumentation, search for suppliers, development of softwares to control the experimental setup, and check of the measurement chain. The present document, which is written at about the ending time of the PRIN grant, is to document all the preliminary phases up to the completion of the experimental setup.
The structure of the document is as follows:

- Chapter 1 is devoted to preliminary considerations on determining the geometric characteristics of the helical coil and the flow conditions;
- Chapter 2 describes the components of the experimental setup;
- Chapter 3 presents the final system configuration;
- Chapter 4 outlines the preliminary tests carried out to check the experimental system and in particular the measurement chain.

Chapter 1

Preliminary study

In this chapter the preliminary study of the experimental setup is described. The key parameters, such as the Reynolds number and Dean number, and the geometrical characteristics (curvature ratio, pitch, etc...), defining the flow conditions are discussed.

1.1 Geometry

The curvature ratio

The curvature ratio δ expresses the geometric characteristics of the coil. It can be defined as:

$$\delta = \frac{d}{D_c} \tag{1.1}$$

where d is the pipe internal diameter and D_c is the coil centerline diameter (see figure 1). The amount of curvature can be defined by following a different definition of the curvature ratio (used i.e. in Refs. [9] and [15]) which turns out to be more complex than Eq. (1.1). If R_c is the centerline radius of the coil, r the internal pipe radius, p_c is the coil pitch and $p_s = \frac{p_c}{2\pi}$, the curvature radius and the helix torsion are defined as:

$$\kappa' = \frac{R_c}{R_c^2 + p_s^2}$$

$$\tau' = \frac{p_c}{R_c^2 + p_s^2}$$

The dimensionless parameters are $\kappa = r\kappa'$ and $\tau = r\tau'$. With the coiled pipe that we will use $\kappa \simeq 0.1$, very closed to the curvature ratio given by Eq. 1.1 (differences from the forth decimal number). Significant differences between the two definitions appear at very high pitch values only. For these reasons most of experimental and numerical studies prefer the simpler definition (i.e. [5, 7, 8, 12, 13, 16]).

Our purpose is to perform an endoscopic PIV: a camera endoscope must be put inside the helical pipe to acquire pictures of the flow. This device has a diameter $d_{end} \simeq 10\,mm$ and can heavily disturb the flow. The pipe diameter d has thus to be chosen large enough to minimize the endoscope influence. A good preliminary choice is $d/d_{end} \geq 10$. In this preliminary evaluation we consider a tube with an internal diameter of $100\,mm$ and thickness of $5\,mm$.
Studies reported in literature consider several values for δ, from 0.001 to 0.5. Because secondary flows are amplified with a large curvature ratio, as shown by Fan et al. in [8], we choose a value of $\delta = 0.1$, already considered in [9] and [16]. This value requires a very low D_c, and we shall check *a posteriori* whether or not the mechanical characteristics of the pipe will be compatible with such an high curvature.

The coil pitch

We decide to use a toroidal-like geometry in this experimental study. This solution simplifies the coiled pipe setup, and can be approximately obtained in practice by minimizing the coil pitch p_c. The lowest possible value of p_c corresponds to the external pipe diameter, i.e. $p_c = 0.11\,m$.

The pipe length

The pipe length has to be chosen so that measurements are unaffected by inlet and outlet effects and a fully developed turbulent flow is established. In a straight pipe this condition is reached after approximately 100 pipe diameters. Therefore measurements may start $10\,m$ (more or less 3 wraps) after the pipe inlet. Geometrical considerations allow up to 20 turns, therefore the pipe length is $L \simeq 63\,m$. The exact number of turns will be determined later, according to considerations of tube costs, single hose length and kind of joints, since connecting two hoses could create significant disturbances in the flow.
All these geometrical properties (curvature ratio, pitch and pipe length) should be considered as a first preliminary evaluation and not as constrains, and could change according to the providers' offers.

1.2 Flow conditions

The Reynolds number

We preliminarly decide to work with water. It is now possible to estimate the main characteristics of the flow. The value of Reynolds number should be high enough to ensure a fully developed turbulent flow, but of course many practical considerations suggest to keep it as low as possible.

According to the literature (in particular [9]), a good compromise value, based on bulk velocity and pipe diameter, is:

$$Re = \frac{dU_b}{\nu} \simeq 6000 \tag{1.2}$$

If the working flow is water at ambient temperature the bulk velocity U_b and the mass flow rate q can be calculated as follows:

$$U_b = \frac{Re\,\nu}{d} \simeq 0.07\,m/s \tag{1.3}$$

$$q = \rho U_b A \simeq 0.55\,kg/s \tag{1.4}$$

The Dean number

There are several definitions of the Dean number employed in literature. A typical definition used in experimental and numerical work (i.e. [5,6,12,13]) based on Reynolds number and curvature ratio, is the following:

$$De = \sqrt{\delta} Re \tag{1.5}$$

Some authors (i.e. [8,16]) give preference for theoretical studies to the definition:

$$De = \frac{\sqrt{2\delta} r^3 G}{\nu\mu} = 8 \left(\frac{2d}{D_c}\right)^{1/2} R_e$$

where R_e is the Reynolds number based on pipe radius r and mean axial velocity and G is the pressure gradient along the duct axis.
Using the definition (1.5) we obtain for the Dean number a value of $De \simeq 2000$. This, together with the values of the Reynolds number, curvature ratio and pitch, defines geometry and flow conditions completely.

1.3 Pressure loss

The pressure loss due to the flow in the duct is given by the following equation:

$$\Delta p = \lambda \frac{L}{d} \frac{1}{2} \rho V^2 + K + \rho g \Delta h \tag{1.6}$$

The first terms is the Darcy–Weisbach equation for distributed pressure losses. The coefficient λ depends on the the friction factor f, which for an helically coiled pipe can be evaluated from the following equation (ESDU source [17]):

$$f = \frac{344 \left(\frac{D}{d}\right)^{-1/2}}{\left\{1.56 + \log\left[Re \left(\frac{D}{d}\right)^{-1/2}\right]\right\}^{5.73}} \tag{1.7}$$

with D internal coil diameter. With the preliminary values $d = 0.1\,mm$, $D = 1\,m$ and $Re = 6000$ we obtain $f = 0.0129$ and the distributed pressure loss in the helical coil is $\Delta p_{coil} = 79.65\,Pa$.
The experimental setup is based on a closed loop system (see §2.5), and the return duct has to be considered too. We shall suppose it has a diameter smaller than the main one, to reduce weight and cost. We can consider a return pipe diameter of $45\,mm$ with a length of $5\,m$. In this return duct, velocity and Reynolds number increase: $V_{rd} = 0.36\,m/s$ and $Re_{rd} = 14196.5$. A definition for the friction factor of straight pipe with turbulent flow is given by ESDU [17]:

$$f = \left[3.6 \log\left(\frac{Re}{7}\right)\right]^{-2} \tag{1.8}$$

We obtain $f_{rd} = 0.00705$ and $\Delta p_{rd} = 203.05\,Pa$. The total distributed pressure loss is thus $\Delta p_d = 282.7\,Pa$.
The second term in Eq.(1.6) deals with the concentrated pressure losses due to localized section changes, joints, etc. It is difficult to establish their value at this stage of the project, since the final layout of the coil is not yet determined. However, the velocities involved are so small that the value of K is not expected to be significantly large.
The third term represents the gravitational pressure drop, and in a closed-loop system it does not give any contribution.
As expected, the global pressure losses in the system are not significant, owing to the low water flow velocity.
The coil complete preliminary characteristics are shown in Table 1.3.

Geometrical characteristics		Water flow characteristics	
Internal pipe diameter d $[m]$	0.1	Bulk velocity U_b $[m/s]$	0.07
Pipe thickness $[m]$	0.005	Mass flow rate q $[kg/s]$	0.55
Pipe length L $[m]$	63	Reynolds number Re	6140
Coil centerline diameter D_c $[m]$	1.1	Dean Number De	1942
Coil height $[m]$	2.20	Friction factor f	0.0129
Pitch p_c $[m]$	0.11	Coil pressure loss $[Pa]$	79.65
Wraps	20	Kinematic viscosity ν $[m^2/s]$	$1.14 \cdot 10^{-6}$
Curvature ratio δ	0.1	Density ρ $[kg/m^3]$	999.1

Table 1.1: Preliminary coil characteristics.

Chapter 2

Pipe and instrumentation

2.1 Choice of the helical pipe

For this experimental study the choice of the helical pipe is of capital importance. Our study aims at describing the weak secondary flows near the wall induced by centrifugal forces: neither internal pipe roughness nor geometric deformations of the shape due to bending must disturb these secondary motions.

2.1.1 Wall roughness

When studying Dean-like secondary flows via numerical simulations, it is of course not difficult to consider perfectly smooth walls, i.e. walls $\varepsilon = 0$, where ε is some kind of r.m.s. roughness of the solid wall. In an experimental work, however, a residual roughness is always present. The literature on roughness effects is large and not uniform: at the present level of knowledge we may assume that $\varepsilon^+ = 0.001 \div 3$ is the range of admissible dimensionless roughness (in wall units) if the mean velocity profile in the straight case is considered. The choice of the pipe will be based on this fundamental requisite.
The viscous length δ_ν corresponding to our case can be calculated starting from its definition:

$$\delta_\nu = \frac{\nu}{u_\tau} \tag{2.1}$$

where u_τ is the friction velocity and ν is the kinematic viscosity. u_τ is estimated from numerical simulations, for example [18], which gives, for a straight pipe at $Re = 4900$ (Re based on centerline streamwise velocity and pipe radius):

$$\frac{U_b}{u_\tau} \approx 14 \tag{2.2}$$

Hence:

$$\delta_\nu = \frac{\nu}{u_\tau} = \frac{1.14 \cdot 10^{-6}}{\frac{0.07}{14}} = 2.3 \cdot 10^{-4}\,[m] = 0.23\,[mm] \tag{2.3}$$

A pipe with roughness $\varepsilon = 0.02\,mm$ hence gives $\varepsilon^+ = 0.087$. This amount of roughness, near the lower allowed range, is considered a good compromise.

2.1.2 Sinusoidal wrinkled wall

Sinusoidal waves on the wall influence the flow heavily, as shown among others by Nakagawa and Hanratty in Ref. [19], where the influence of a structured wavy wall on turbulence is studied. We can assume the same important influence on a coiled pipe flow, and in particular on the secondary Dean flows. It is reasonable to imagine that a large sinusoidal disturbance can destroy such structures. We could accept wavy wall with small amplitude lower than $0.5\,mm$, according to [19].

2.1.3 Realization of the pipe

The pipe can be assembled by following two different solutions: a metallic helical tube can be used, or a flexible tube. Obviously both solutions present advantages and disadvantages. We discuss them here.
A metallic coiled pipe, madeby aluminium or stainless steel, certainly represents a good choice. There are factories producing such items, both in Italy [20] and in the U.S.A. [21–24]. Metallic coiled pipes can have a very small roughness and simplify the experimental setup. In fact we would not have to fix the coil, because it would have its own supports for vertical positioning; the circular shape of the pipe section would be preserved for all the pipe length without the need for external supports (saddles). If an appropriate thickness (more or less $4\,mm$) is available, seals could be made directly on the pipe, without external supports. In alternative a smaller thickness could be used to keep the coil weight low and very simple saddles could be used to obtain seals. A metallic pipe allows an arbitrary predetermined coil pitch. We could thus easily design our pipe to work in an actually helical geometry instead of a toroidal geometry. Obviously the wrap number should be reduced, to keep coil height and weight under control.
For the coil to preserve circular cross-section without ovality under curvature, coil dimensions larger than those estimated previously are needed. In particular the coil diameter should be increased, and a too small pipe thickness should be avoided. A reasonable metallic helical pipe would have the dimensions shown in Table 2.1.

	Values in *in*	Approximate values in *mm*
Pipe internal diameter	4	101.6
Thickness	0.237	6
Coil centerline diameter	60	1524
Coil height	120	3048
Pitch	8	203.2
Full wraps	15	15
Material	stainless steel	stainless steel

Table 2.1: Typical dimensions of a workable metallic coiled pipe.

Disadvantages of this solution are both technological and economical. The coiled pipe is factory-made by bending straight tubes and then soldering them together: *a priori* the welding quality cannot be guaranteed nor known, and the localized welding could disturb the water flow and disturb the Dean structures. The stainless steel straight tube maximal length is $6\,m$, so that one welded section for each wrap would be needed. Moreover, the coil pitch, however freely choosable, cannot be changed for future different experimental campaigns. Another problem is related to the cost of the . This solution, in fact, is expensive. For example the metallic coil described in Table 2.1, with external supports, has a price of about US$ 22000 (source [21]). Decreasing the dimensions (from $4\,in$ to $3\,in$ for the internal pipe diameter) does not reduce the costs significantly. The Italian producer [20] is cheaper, and can provide the coil for a price of about € 5200.
An alternative choice for pipe realization is the use of flexible, rubber- or PVC-made pipes. The main problem here is related to the pipe roughness. With our required diameter, rubber tubes do not ensure the required internal smoothness due to manufacturing imperfections (not important for industrial applications but critical for us), that get larger and larger in tube with larger diameter. Another problem is maintaining the required circular section shape. In fact, under mechanical load, pipe sections could undergo large deformations. Tubes with one or more PVC or steel spirals inserted in their thickness overcome the latter problem and warrant relatively low-curvature radius. However such spirals might determine sinusoidal imperfections on the internal walls, that might carry bad consequences. Polyethylene tubes, with an extremely smooth internal surface and without spirals, allow a too large curvature radius (more or

	Values in mm
Pipe internal diameter	102
Thickness	8
Coil internal diameter	900
Coil centerline diameter	1018
Coil height	1475
Pitch	118
Wraps	12.5
Material	rubber

Table 2.2: Dimensions of the used helically coiled pipe.

less $2.5\,m$) and cannot be used for the present experiment.
The optimal solution comes from a food-grade pipe equipped with two internal steel spirals, put in a rubber layer inside the pipe thickness and manufactured on a chromium-plate mandrel. This should overcome all the previous problems. This pipe has been provided by Giacomo Abbadini & C. SAS [25]. The main characteristics of the pipe are reported in Table 2.2. The pipe is then wrapped on a steel cylinder with a $0.9\,m$ external diameter, $4\,mm$ of thickness and $2\,m$ of height. Because the tube is provided in a $40\,m$ hose, we decided to reduce the wraps number down to 12.5 (preliminary evaluation was based on 20 turns), so avoiding the need for connection between hoses.
The experiments are performed in a closed-loop system (see §2.5). For the return duct an extremely smooth pipe is not necessary. A cheaper tube, smaller than the first one, can be used. We use a PVC tube, named Armo, with $45\,mm$ of internal diameter and $5\,mm$ of thickness and characterized by an internal steel spiral (see Figure 2.1).

2.1.4 Tube joints

The $102\,mm$ inner diameter of the main pipe has to be connected to the $45\,mm$ inner diameter of the return duct pipe. The two tubes have been connected through section reducers. Joints are moreover needed to connect the return duct pipe to the pump, both at the inlet and at the outlet. A tee-joint has been moreover installed to allow for seeding the flow with particles. Another tee-joint coupled with a spherical valve makes the drain system of the water circuit.

Figure 2.1: The PVC Armo tube used for the return duct.

2.2 The actual coil

Once the pipe has been chosen, the actual geometrical and fluidodynamic characteristics of the coil have been re-evaluated, and they are presented in Table 2.2. No important changes have been introduced with respect to preliminary evaluations (compare to Table 1.3) except for the pipe length and therefore for the number of wraps. The choice of a shorter pipe is motivated by the difficulty of joining two hoses without significantly affecting the smoothness of the water flow. We have thus decided to reduce the wrap number while preserving the internal smoothness of the surface. Anyway, the lower value of 12.5 turns should allow one to measure without inlet and outlet effects and with a fully developed turbulent flow. The coil diameter is dictated by the pipe mechanical properties, and a curvature ratio very close to the required one can be obtained.
The pressure drop is affected by joints, which cause concentrated losses, that are evaluated thanks to a handbook of hydraulic like Ref [26]. However, because of the small flow speed, they do not significantly increase the global pressure drop of the system (see Table 2.4), that are increased to $\Delta p = 602.05\ Pa$ only.

2.3 Control of the flow speed

Measuring and controlling the flow speed in the helical coil is a required ability in order to be able to set the value of the Reynolds number

Geometrical characteristics		Water flow characteristics	
Internal pipe diameter d $[m]$	0.102	Bulk velocity U_b $[m/s]$	0.07
Pipe thickness $[m]$	0.008	Mass flow rate q $[kg/s]$	0.572
Pipe length L $[m]$	40	Reynolds number Re	6263.16
Coil internal diameter D $[m]$	0.9	Dean Number De	2038.81
Coil centerline diameter D_c $[m]$	0.959	Friction factor f	0.0131
Coil height $[m]$	1.475	Coil pressure loss $[Pa]$	50.34
Pitch p_c $[m]$	0.118	System pressure loss $[Pa]$	602.05
Wraps	12.5	Kinematic viscosity ν $[m^2/s]$	$1.14 \cdot 10^{-6}$
Curvature ratio δ	0.106	Density ρ $[kg/m^3]$	999.1

Table 2.3: Characteristics of the used coil.

correctly. We measure at the pipe wall the differential pressure on the upstream and downstream sides of an orifice plate inserted into the duct. Differential pressure is related to flow rate, and therefore to flow speed, by discharge coefficient; they are tabulated in ISO norms for a well defined geometry of the orifice plate. Knowledge of the pressure drop thus leads easily to the flow speed. An additional advantage of measuring the flow speed through this configuration is that the additional pressure drop due to the orifice plate serves an useful purpose, since it helps dampening disturbances in the flow and obtaining a better operating point for the pump.

Following the ISO norm [1], a flowmeter has been designed and realized on purpose. It is characterized by an orifice plate of 38 mm diameter and 2 mm thickness, with a single hole concentric with the pipe centerline of 13 mm diameter (see Figure 2.2). The orifice size cannot be too small, because the tiny particles added to water for PIV might heap and stop there. For a particle diameter of 10 μm the orifice size is 1300 times larger, and no problems are expected. The local pressure loss due to the plate is about 25000 Pa (25126.52 Pa), therefore the system pressure loss increases to $\Delta p \simeq 25728.17\, Pa$ (with a head loss $H = 2.62\, m$).

The flowmeter is built with two aluminium tubes with an internal diameter $\phi = 38\, mm$ and thickness $s = 5\, mm$. Aluminium flanges glued on them have been used to connect and to place the orifice plate in the right

[1] Evaluation of flow rate and pressure loss due to the orifice plate has been done using the British Standard EN ISO 5167–1:1997, "Measurement of fluid flow by means of pressure differential devices".

	Pressure loss $[Pa]$
Main pipe	50.34
Return duct	203.05
Joints	
Section reducer	244.98
Section increaser	71.28
Two tee-joints	32.4
Tot.	601.45

Table 2.4: Pressure loss in the system.

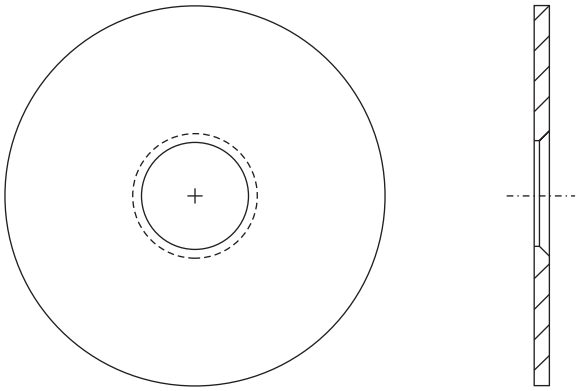

Figure 2.2: Sketch of the orifice plate.

position. The position of the pressure tapping positions is dictated by the ISO norms: nominally ϕ upstream of the plate and 0.5ϕ downstream, as shown in Figure 2.3.

Absorbed power

It is useful to estimate the mechanical power needed to win the pressure loss. This power is dissipated into heat, and this increases the water temperature while the system is on, so decreasing its viscosity and therefore modifying the value of the Reynolds number at constant speed. An heat exchanger might be required to keep a constant temperature. The power absorbed by the fluid is given by:

$$\mathcal{P} = q_v \Delta p = 14.75\, W \tag{2.4}$$

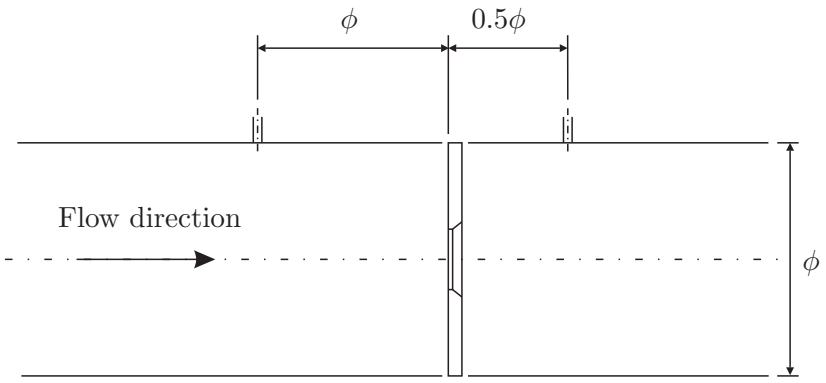

Figure 2.3: Spacing of pressure tappings for the orifice plate.

where q_v is the volumetric flow rate express in m^3/s and Δp the global pressure drop in the system due to both distributed and concentrated pressure losses. The increase of temperature can then estimated with an energetic balance:

$$Q = mc_p\Delta T \tag{2.5}$$

where $Q = 53122.2\,J$ is the energy supplied to the fluid in one hour, $m = 340\,kg$ the mass of water flowing in the system and $c_p = 4186\,J/kgK$ the specific heat of water. We obtain an increase of temperature of $0.0373°C$ after a one-hour run. This low value does not significantly affect the water viscosity during the measurements: the viscosity decreases of about 0.097% after one hour. An heat exchanger is therefore not required, even in case of longer runs. An accurate measurement of the water temperature is however mandatory.

2.4 Digital camera

For PIV applications a special camera is needed to record two images with a small interframing time. A Pixelfly Double Shutter camera (Figure 2.4) provided by PCO [27] is used, with a CCD size of $1280 \times 1024\,pixels$, which allows different operating modes: video, asynchronous and double shutter mode. The last one is that required by PIV applications. Recording images from inside the helical pipe while keeping the related flow perturbations to a minimum requires an endoscope probe. A rigid device with a diameter of $8\,mm$ and a viewing field of 40° has been used. The device can also be used with an optional mirror of $8.5\,mm$ diameter for a 90° direction of view.

Figure 2.4: The Pixelfly Double Shutter camera.

2.4.1 Camera control

The camera control is limited at the operation mode, the exposure time and the trigger mode (internal or external). No other parameters can be set. In particular it is not possible to choose when the second image for the double shutter mode has to begin and its exposure time. In fact this time corresponds to the readout time of the first image, as we can see in Figure 2.5 where the camera work diagram (Busy, CCD–Exposure time and CCD–Readout time signals) supplied by the provider is presented. This diagram contains several inaccuracies in the timing information, so that we had to measure them avain with an oscilloscope to obtain reliable data.
The correct time exposure and the beginning of the second image will be set by the intensifier unit and its parameters.

2.4.2 Interframing time

It is important to estimate the time t_p taken by a single particle to pass through the laser beam thickness. The time between two consecutive photograms must be less than t_p, so that most of the particles inside the laser thickness at the time of the first photogram, will still be there at the time of the second one, thus making correlations between the two pictures possible. The estimate of t_p is based on the bulk velocity U_b and the laser beam thickness s_l, that can be considered of 1 mm:

$$t_p = s_l/U_b = 0.001/0.07 \simeq 0.015\, s = 15\, ms \tag{2.6}$$

It is now necessary to choose the size of the field of view. Particle

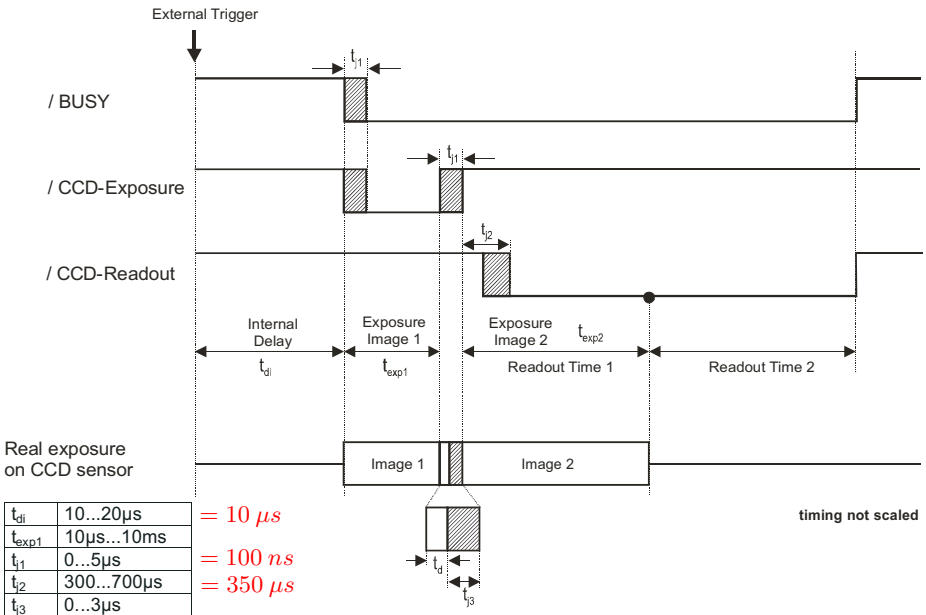

t_{di}	10...20µs
t_{exp1}	10µs...10ms
t_{i1}	0...5µs
t_{i2}	300...700µs
t_{i3}	0...3µs
t_d	2µs

Figure 2.5: Camera signals in double shutter mode (provided by PCO [27]) with our measurements of the time inaccuracies (red color).

displacements must be 1 *pixel* at least to be appreciated from two consecutive camera pictures. A large field (for example $50 \times 50\,mm$) does not let us detect any particle movement, due to the small secondary flow velocity in the cross-section. In fact, it would be necessary a long time interval between two photograms to see a particle displacement. But during this time the particles would pass through the whole laser thickness (crossing time of 15 ms, see Eqn. (2.6)), and would thus be absent in the second photogram. The laser beam thickness should be increased to increase the crossing time. In our case, however, the thickness cannot exceed $1 - 2\,mm$, therefore the dimensions of the field of view must be reduced. A reasonable size is $10 \times 10\,mm$. With a $1280 \times 1024\,pixel$ CCD size and $10 \times 10\,mm$ field size, we have that $1\,pixel \simeq 0.01\,mm$. A typical value of velocity for the secondary flow can be considered $u = 0.03U_b$, according to Lin and Ebadian in [7]. The time Δt taken by a particle with speed u to move of 1 *pixel* is:

$$\Delta t = \frac{\Delta x}{u} = \frac{0.01 \cdot 10^{-3}}{0.03 \cdot 0.07} \simeq 0.0047\,s = 4.7\,ms \tag{2.7}$$

A good interframing time is thus 6 ms, that allows to see displacements most of the particles, which remain inside the laser beam thickness for the two consecutive photograms.

2.5 Seeding particles

Fluorescent particles are a great solution for PIV applications, because they can enhance the signal-to-noise ratio. Such particles emit distinctive colors when illuminated by wavelengths shorter than the emission wavelength. This property improves their contrast and visibility relative to background material, so that they have an improved detectability with respect to the conventional microspheres. To achieve this goal the optics of the receiving device must be equipped with a suitable optical filter, centered on the corresponding wavelength. In particular a 3^{rd} Millennium bandpass filter product by Omega Optical [28] with 580 nm as cut-on value and 660 nm as cut-off could be used in our setup.
Particles based on polystyrene are well suited to our application, because their mass density is 1.05 g/cm^3, very close to the density of water. Moreover fluorescent dye with excitation wavelength for green laser source, required for applications in water, is necessary (typically rhodamine). The experiments can be performed in a closed-loop or in an open-loop system. The latter choice permits a simpler setup, but the particles in the water flow (very expensive as can be appreciated from Table2.5) would be lost. Hence a closed-circuit solution has been preferred.

	Diameter [μm]	Type	Price
Distrilab[1] (Netherlands)	5, 10, 15	Dry	205 €/g
LaVision (Germany)	20–50	Dry	110 €/g
Kisker–Biotech (Germany)	10.2	Suspension (1%)	117.5 €/ml
	15	Suspension (1%)	129.5 €/ml
	20	Suspension (1%)	120 €/ml
Spherotech (U.S.A.)	10–14	Suspension (1%)	87.5 US$/$ml$
	15–19	Suspension (1%)	100 US$/$ml$

[1] distributor for Europe of Duke Scientific Corporation.

Table 2.5: Price of some fluorescent particles.

2.5.1 Estimating the required numbers of particles

We estimate here the approximate amount of seeding particles and their size. Fluorescent particles are expensive and using a small amount of them saves significant money. A 10 μm particle diameter could be a good solution. In the correlations for the PIV, interrogation windows of $128 \times 128\, pixel$ can be used (according to [29]), corresponding to a physical spatial resolution of approximately $1\, mm$ (the dimensions of the field of view is $10 \times 10\, mm$, as estimated in §2.4). It can be assumed that a good particles amount is twenty particles per window, therefore in our case $20\, p/mm^3$.
The approximate total water volume is given by the helical pipe volume ($d_{in} = 102\, mm$, $l = 40\, m$) and the return duct volume (Armo tube: $d_{in} = 45\, mm$, $l = 5\, m$):

$$V_{tot} = V_{coil} + V_{rd} = 40\pi \left(\frac{0.102}{2}\right)^2 + 5\pi \left(\frac{0.045}{2}\right)^2 \simeq 0.34\, m^3 \qquad (2.8)$$

Particle total number is:

$$N_p = 20 \cdot 0.34 \cdot 10^9 = 6.8 \cdot 10^9 \rightarrow 7 \cdot 10^9 \qquad (2.9)$$

Nominal diameter	$10\,\mu m$
Mean diameter	$8\,\mu m$
Size uniformity (CV)[1]	14%
Density	$1.05\,g/m^3$
Refractive index	1.59 @ $589\,nm$
Material	Polystyrene Divinylbenzene (PS-DVB)
Fluorescent dye	Ex. max 542 / Em. max 612 nm
Number/gram	$1.8 \cdot 10^9$

[1] Coefficient of Variation (CV) is the size distribution (standard deviation).

Table 2.6: Characteristics of the used fluorescent microspheres.

To estimate the necessary volume of particles we suppose that they probably will be clumped each other, therefore we can assume that they have a square shape with a $10\,\mu m$ size. The volume of one particle will be:

$$\mathcal{V}_p = (10 \cdot 10^{-6})^3 = 10^{-15}\,m^3 = 10^{-6}\,mm^3$$

The global particles volume required is[2]:

$$V_p = N_p \cdot \mathcal{V}_p = 7 \cdot 10^9 \cdot 10^{-6} = 7 \cdot 10^3\,mm^3 = 7\,ml \simeq 7\,g \tag{2.10}$$

With this amount of particles a dilute suspension flow with a tracer particle volume fraction of $2.05 \cdot 10^{-5}$ is obtained.
The fluorescent particles (Duke Scientific Corporation 36-3) have been acquired by Distrilab BV [30]. Their main characteristics are listed in Table 2.6, where in particular the excitation/emission properties re reported: absorption maxima at a wavelength of $542\,nm$ (this corresponds at the excitation maxima) and emission maxima at $612\,nm$. The number/gram figure confirms the previous estimate of the required amount of particles.
The microspheres are packaged as dry and must be suspended before using. The provider gives a simple procedure to obtain a diluted suspension:

[2] If the previous approximation is not used for the particle volume, we have:

$$\mathcal{V}_p = \frac{4}{3}\pi(5 \cdot 10^{-6})^3 = 5.23 \cdot 10^{-7}\,mm^3$$

and therefore:

$$V_p = N_p \cdot \mathcal{V}_p = 3.661 \cdot 10^3\,mm^3 = 3.661\,ml \simeq 3.661\,g$$

A value which is half of the approximated amount of necessary particles.

1. wet dry particles with a 1% surfactant solution (anionic or non-ionic) or an alcohol such as methanol or ethanol;

2. add filtered water to the desired amount.

2.6 The laser source

In PIV techniques a pulse laser is usually employed. This device produces a very high power beam and allows one to obtain consecutive pictures with an imposed interframing time. The price for a pulse laser is very high tough (US$ 40000 or more), and a green pulse laser, which is required for applications in water, most probably will not be used anymore for future projects, whereas an infrared source (suited for air applications) is deemed to be more useful for measurements in the wind tunnel. For these reasons we have decided to use the pre-existing not-pulsed green laser, and to purchase an intensifier unit, to obtain a pulse-like output. The employed laser is a Spectra–Physics Stabilite 2017 Series argon laser, which transmits a single-line beam at 514.5 nm with a power of 2.0 W. The laser source characteristics are shown in Table 2.7.
To bring the laser beam inside the pipe a rigid endoscopic illuminator of 8 mm diameter has been used, which produces a laser blade of 60°. This device too can be used with a mirror for a 90° lighting.

2.7 Synchronization unit

The synchronization unit is a pulse generator needed for controlling and timing camera and intensifier unit. It is connected to the controlling Personal Computer by a serial port, and driven by a Labview software. The synchronizer used is model QC9618 provided by Oxford Lasers [31]. This device has two timers, the System Timer and the Channel Timer, needed to generate the required output. Its working scheme is presented in Figure 2.6: once the device is started, a signal (start pulse) arms the internal System Timer, and an internal pulse with imposed period T_o is generated and sent to the Channel Timer which routes the output pulses to the selected channels. The System Timer functions as a non-retriggerable, multi-vibrator pulse generator. This means that once started the timer produces pulses continuously. Before pulses are generated, the timer must be armed and then receive a start pulse. Once the System Timer is started, the counter operation is determined by the System Mode Generator. Standard operating modes include:

- continuous: T_o pulses are generated continuously;

- single shot: one T_o pulse is generated for each start command;

Output characteristics	*Stabilite 2017 –AR*
Multiline output power	
333.6–363.8 nm (UV)	100 mW
457.9–514.5 nm (Vis)	6.0 W
Single–line output power	
454.5 nm	100 mW
457.9 nm	200 mW
465.8 nm	120 mW
472.7 nm	170 mW
476.5 nm	450 mW
488.0 nm	1.5 W
496.5 nm	600 mW
501.7 nm	300 mW
514.5 nm	2.0 W
Beam diameter at $1/e^2$ points	1.4 mm
Beam divergence	0.5 $mrad$
Polarization	100:1 vertical
Optical noise, current mode	$\leq 0.5\%$ rms
power mode	$\leq 0.5\%$ rms
Power stability, current mode	$\pm 1\%$
power mode	$\pm 0.5\%$
Beam pointing stability	≤ 7.5 $\mu rad/^{\circ}$C

Table 2.7: Spectra–Physics Stabilite 2017 series argon laser technical characteristics.

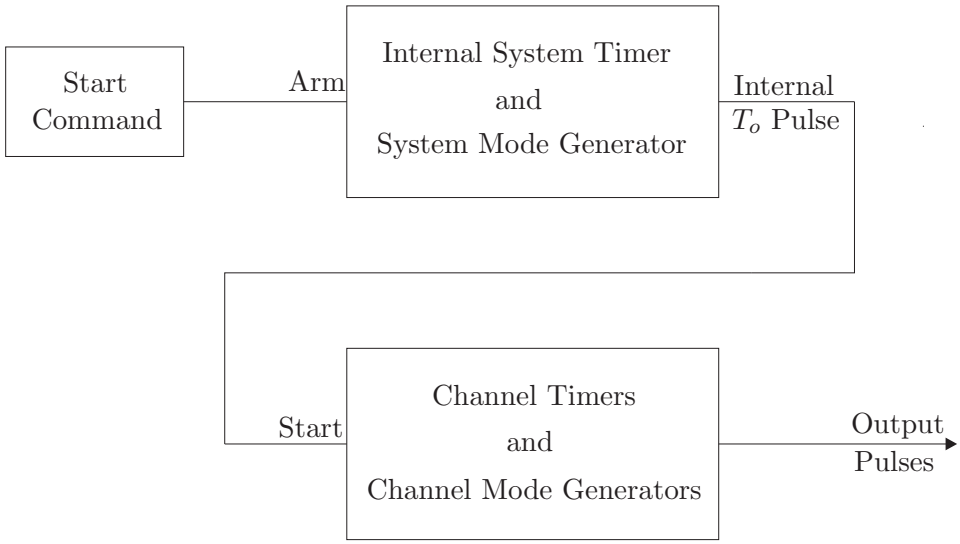

Figure 2.6: The architecture of the synchronization unit.

- burst mode: n pulses with period T_o are generated for each start command;
- duty cycle: T_o pulses cycle on and off continuously.

The Channel Timer works as a non-retriggerable, delayed, one shot pulse generator. This means that the timer can only generate one delayed pulse for every received start pulse. Once the channel timer has started counting, additional start pulses will be ignored until the pulse has been completed. The start pulse for each channel is provided by the internal T_o pulse generated by the internal System Timer. Whether or not a pulse is generated for each T_o pulse is determined by the Channel Mode Generator. Standard operating modes include:

- normal: a pulse is generated for each T_o pulse;
- single shot: one pulse is generated at the first T_o pulse, after which output is inhibited;
- burst: a pulse is generated for each T_o pulse, n times, after which output is inhibited;
- duty cycle: a pulse is generatedfor each T_o pulse n times, after which the output is inhibited for m times. The cycle is then repeated.

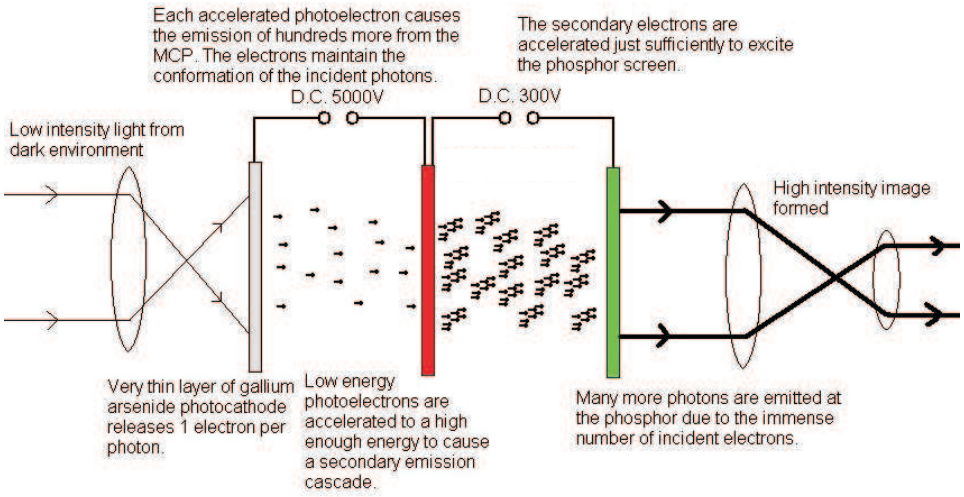

Figure 2.7: How the image intensifier unit works.

2.8 Image intensifier unit

The high brightness required to obtain pictures of seeding particles is obtained with the continuous laser beam thanks to the amplification of the laser beam. This is accomplished by an intensifier unit used to this aim. The intensifier unit serves moreover the additional use of obtaining two consecutive PIV images taken at an arbitrarily small interframing time, thanks to its gate time unit. Indeeed, the initial time and the exposure time of the second picture cannot be controlled by the camera (see §2.4). An image intensifier is a device that intensifies an image with light levels to light levels that can be appreciated by the human eye, or detected by a digital camera. An image intensifier is basically a vacuum tube, which carries an input window where a light-sensitive layer, called photocathode, has been deposited. Photons are absorbed in the photocathode and emit electrons to the vacuum. These electrons are then accelerated by an electric field to increase their energy and at the same time focus them. After multiplication by an MCP (Multi-Channel Plate), in a process called secondary cascaded emission, these electrons are eventually accelerated towards the anode screen. This screen contains a layer of phosphorescent material covered by a thin aluminium film. When an electron hits the anode, its energy is converted into photons again. Because of the multiplication and the increased energy of the electrons, the output brightness is now higher compared to the original input light intensity (see Figure 2.7).
The intensifier used is the C9548 series provided by Hamamatsu

Photonic [32]. It has been connected to the controlling Personal Computer by a serial port, and is driven by a Labview software.

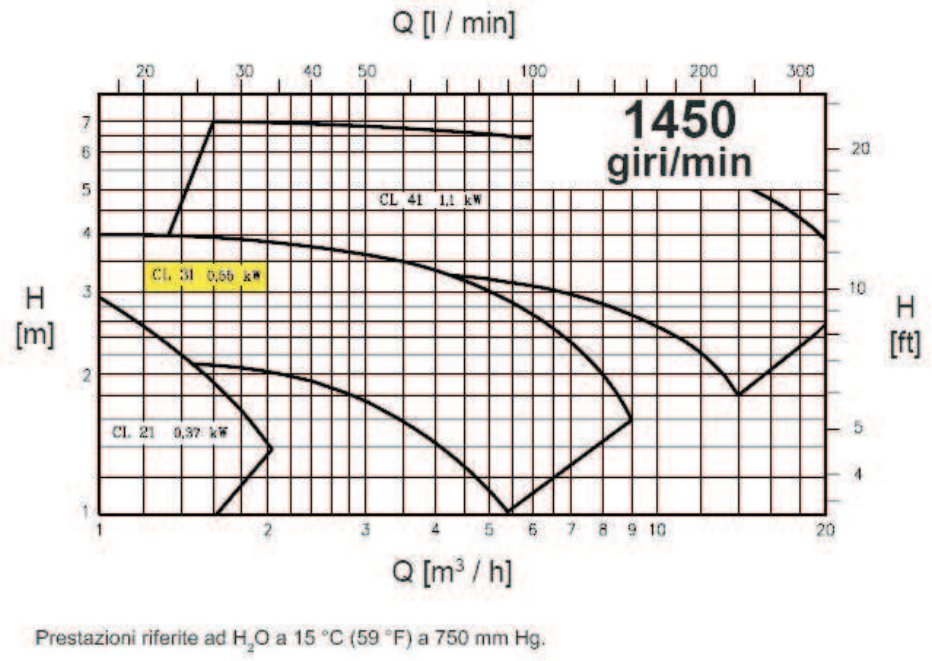

Figure 2.8: The pump working diagram (source CSF Inox [33]).

2.9 Other instruments

The experimental setup is completed by other instruments that will be briefly described below.

Pump

The pump is necessary in the closed-loop system. Easy dismantling for inspection and cleaning from residual particles present in the water flow are important pump requirements. Food-grade pumps do satisfy these requests. Moreover the pump should not disturb the flow. For removing any swirling motion a honey-comb has been installed (size $d = 3\,mm$ and $l/d = 10$). Its best position is after the pump outlet, where most of the vorticity due to the pumping device is concentrated.
The pump used is the centrifugal pump CL–31 series provided by CSF Inox S.p.A. [33]. In Figure 2.9 its working diagram is shown. The orifice plate of the flowmeter gives a concentrated pressure loss that makes the pump operate well inside its working range ($q = 2\,m^3/h$, $H = 2.62\,m$).

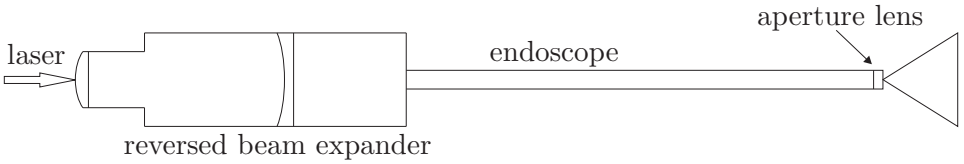

Figure 2.9: Schematic drawing of the laser endoscope.

Endoscopes

As described in the previous sections (§2.4 and §2.6) two rigid endoscopes are used in our endoscopic PIV setup. Their main characteristics are listed here.
The first endoscope is required to allow the camera record inside the pipe. This device has a diameter of 8 mm and allows a viewing field of 40° degree with a 0° direction of view. An optional mirror can be mounted for a 90° direction of view, which increases the endoscope diameter to 8.5 mm. This endoscope has been provided by TRE–I Fibre Ottiche [34].
An endoscopic illuminator is also required to bring the laser beam inside the pipe and to light the fluid flow. The setup of the laser endoscope is shown in figure Figure 2.9. It has a diameter of 8 mm and allow us to obtain a laser blade of 60°; a mirror for a 90° viewing direction can be also mounted. The aperture lens at the outlet of the tube consists of a cylindrical lens, and a reversed beam expander is used to decrease the laser beam diameter. This second endoscope has been provided by FluxOptica S.r.l. [35].

2.10 Suppliers

In the following table the purchased products and their suppliers are listed.

Product	*Main characteristics*	*Supplier*
Main pipe	$d_{in} = 102\,mm$ $s = 8\,mm$ $L = 40\,m$ material: rubber	Giacomo Abbadini & C. [25]
Return duct pipe (Armo)	$d_{in} = 45\,mm$ $s = 5\,mm$ material: PVC	
Joints	material: bronze, cast iron (tee-joints only)	
Pump (CL–31 series)	centrifugal pump $power = 0.55\,kW$	CSF Inox [33]
Intensifier unit (C9548)	$gain = 600 - 1000$	Hamamatsu Photonic [32]
Camera (Pixelfly Double Shutter)	CCD size: 1280×1024 $t_{exp} = 10\,\mu s - 10\,ms$	PCO [27]
Synchronizer (QC9618)	$resolution = 10\,nm$ $pulsewidth = 10^{-8} - 1000s$	Oxford Lasers [31]
Camera endoscope	$d = 8\,mm$ $viewing\ field = 40°$ mirror for a 90° viewing $(d = 8.5\,mm)$	TRE–I Fibre Ottiche [34]
Laser endoscope	$d = 8\,mm$ $laser\ blade\ field = 60°$ mirror for a 90° illumination	FluxOptica [35]
Particles	$d = 5 - 35\,\mu m$ material: polyamide 12	Dantec Dynamics [36]

Fluorescent particles	$d_{mean} = 10\,\mu m$ material: polystyrene PS-DVB dye: red fluorescent	Distrilab [30]
Extension tube set	set of six rings	Sicurit Alarmitalia [37]
Steel cylinder	size: $900 \times 2000 \times 4\,mm$	M.M. Montanari Massimo [38]
Iron plate	size: $1000 \times 2000 \times 4\,mm$	Italfer Folzini [39]
Aluminium tube	$d_{in} = 38\,mm \quad s = 5\,mm$	Migliari Alluminio [40]
Flanges	type: FF-A6 PN6 DN40	Fonderia Fazzini [41]
Acrylic rods	$d = 8\,mm$ and $d = 4\,mm$	La Politecnica [42]
Manufacturing	laser/endoscope interface	UTP [43]

Table 2.8: Purchased products and their suppliers.

Chapter 3

Experimental setup

In this chapter the configuration of the whole experimental system is briefly described.

3.1 The measurement chain

The instrument connection follows the scheme sketched in Figure 3.1. As we can see the camera is directly connected on one side to the controlling Personal Computer by a PCI board, and on the otehr side to the intensifier unit to the pulse generator, which in turn connects to the PC via a serial port. Through its PCI board, the camera is also connected to the pulse generator, which synchronizes this device and the intensifier unit. This allows to record pairs of frames with an imposed interframing time, which has to be chosen based on the flow characteristics. The connection scheme of the acquisition instruments is shown in Figure 3.1, where a relay lens is interposed between camera and image intensifier. All the instruments (camera, pulse generator and image intensifier) are controlled by softwares developed in the LabView programming language.
The camera must trigger the system, because its board initialization gives some signals before the exposition of the first photogram. This device gives the trigger input (after its board initialization) to the synchronizer. There are now two possible configurations. In the first one the synchronizer generates two pulses, with imposed width and period, which activate the intensifier unit. This device produces one exposition at each pulse. Alternatively, the synchronizer may send one pulse only to the intensifier, which responds with two expositions, at a given time interval. In any case, it is required that the first intensifier exposition cohincides with the first camera exposition and the second one is during the second camera exposition, according to the interframing time (see §2.4). We have decided to use the first configuration.

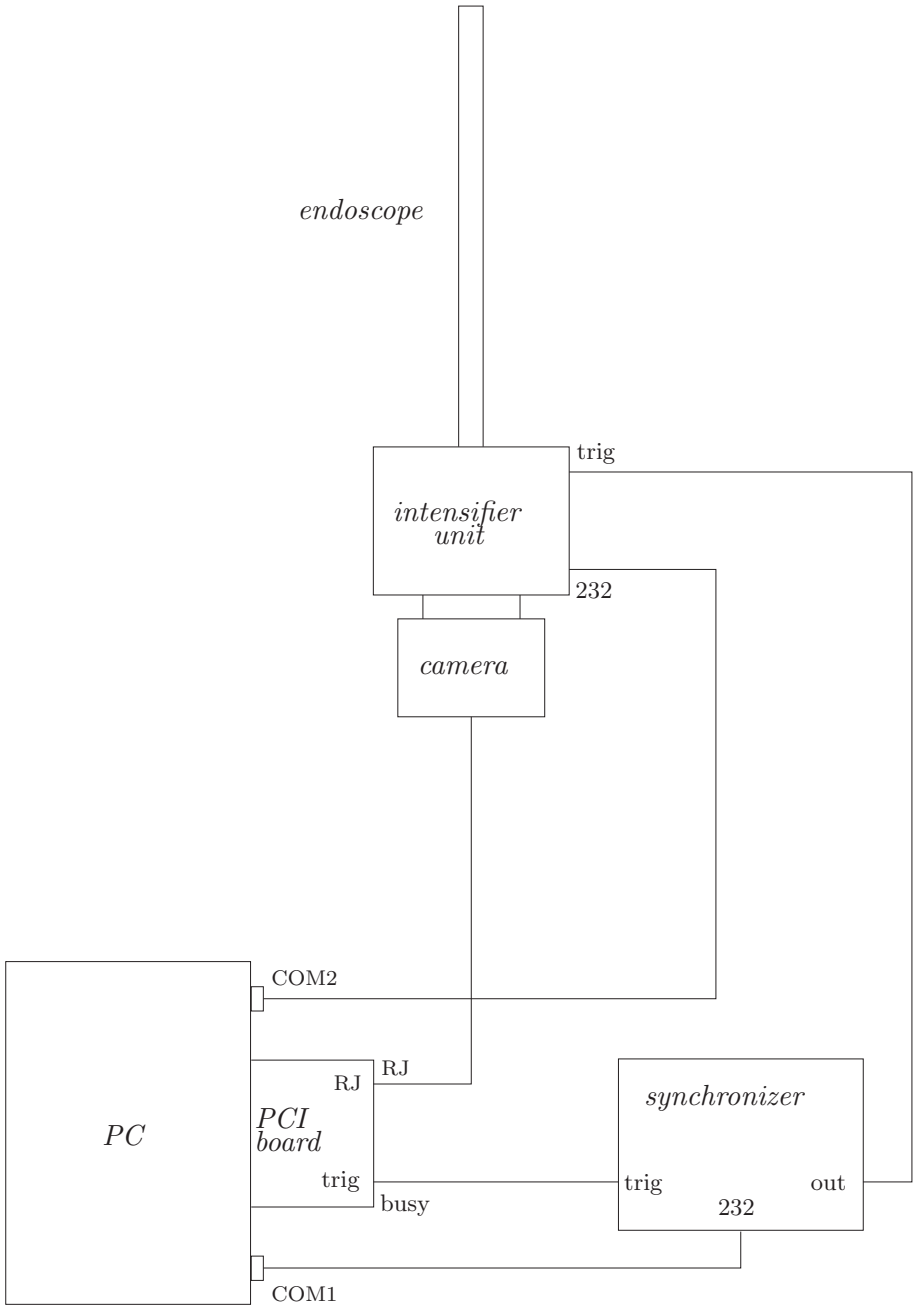

Figure 3.1: The instruments communication scheme.

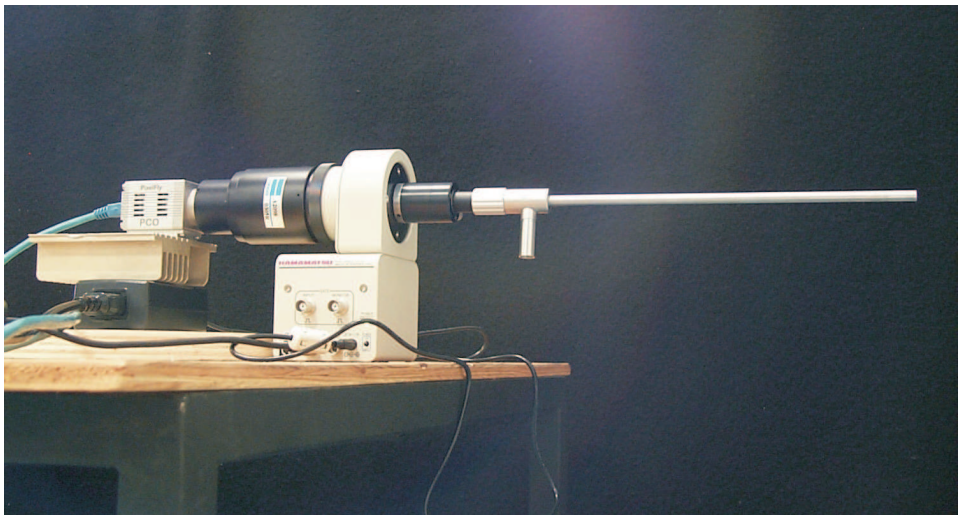

Figure 3.2: The acquisition system is composed by an endoscope, the image intensifier unit with its relay lens and the camera.

3.2 Measurements

In the preliminary design, measurements in the bottom half of the wraps were considered. Along the development of the project, we have taken the decision of measuring in the last turn only. This choice grants easier access to the pipe, because the endoscopes can be mounted in vertical position (see Figure 3.3). Above all, this setup allows detecting both streamwise and cross section velocity field with the suitable endoscopes. For the former the 90° laser endoscope and the 0° camera endoscope must be used. For the latter, 0° for the laser endoscope and 90° mirror for the camera endoscope, as shown in Figure 3.4.

3.3 System frame

A frame is required to maintain the coil in the corrrect position, with the imposed geometrical characteristics (pitch and curvature ratio) and to link all the system parts (flowmeter, saddles for the endoscopes, pump, instruments, ...).
The structure we have built is based on metallic parts, painted to prevent rust. A steel cylinder has been welded on a iron plate (size $1000 \times 2000 \times 4\,mm$). The cylinder has an external diameter of $0.9\,m$, thickness of $4\,mm$ and height of $2\,m$. It is required to support the coil in the correct position with the imposed curvature ratio ($\delta = 0.1$). In this cylinder two windows of $0.15 \times 0.4\,m$ at about 180° each other have been

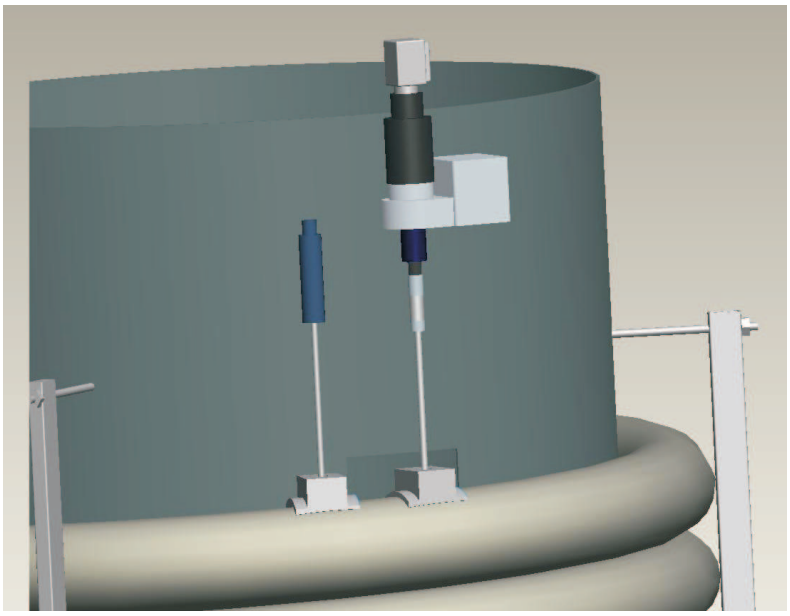

Figure 3.3: Setup of the system acquisition: the instruments are mounted in vertical position and the measurement section is in the last wrap.

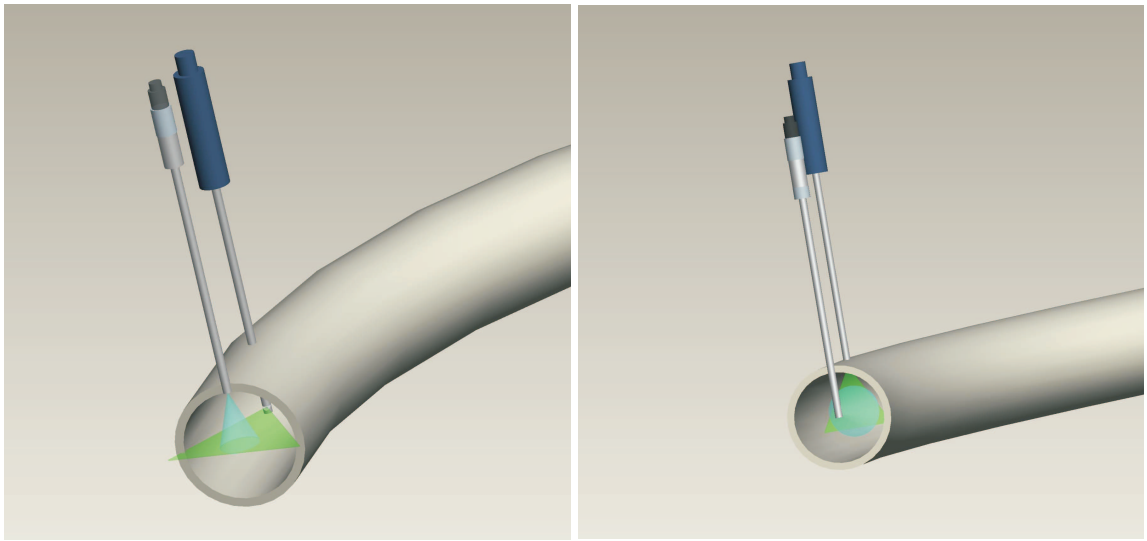

Figure 3.4: The two possible endoscopes configurations, which allow to detect the velocity field both in the streamwise direction (a) and in the cross section (b).

Figure 3.5: The coil frame.

cut for future internal measurements. Three iron bars at 120° each other help keeping the pipe attached to the cylinder: they have been very helpful during the lengthy procedure of wrapping the pipe around the coil core. At the lower end of the cylinder six plywood supports have been pasted on the plate in order to impose the correct pitch of the first wrap of the pipe. In Figure 3.5 the coil frame with the plywood supports cab be seen.

Figure 3.6: The helical pipe system.

Chapter 4

Some preliminary tests

Before starting the real experiments in the helical coil turbulent flow, preliminary tests have been carried out to check instrumentation, softwares, the measurement chain. This has given the opportunity of verifying some crucial evaluations of the preliminary phase.

4.1 What can be measured?

The lowest particles dimension and the viewing field problem

It is obviously very important to be sure of the lowest particle dimension that can be detected with the camera. To check this, we have arranged a simple test where a B/W drawing with either four lines per millimeter and eight lines per millimeter has been put in front of the camera. The endoscope was at a distance of about $15 - 20\,mm$, thus very close to the conditions of the future experiments. As shown in Figure 4.1 both kind of lines can be clearly seen. With eight lines per millimeter, each line is $125\,\mu m$ apart from its neighbour. From the picture we estimate that the mean thickness of a single line is around $20\,pixel$. We educe that we should be able to detect particles of $6 - 7\,\mu m$ of diameter. This is in accordance with our preliminary choice of seeding particles with a $10\,\mu m$ diameter (see §2.5).
Figure 4.1 gives an important information about the field of view. As can be seen, it is around half than the possible: the CCD size is $1280 \times 1024\,pixel$ against the $550\,pixel$ field radius. This is because the endoscope and image intensifier unit are too close. Extension tubes, that are being acquired, will be evaluated for moving them away and so increasing the viewing field.

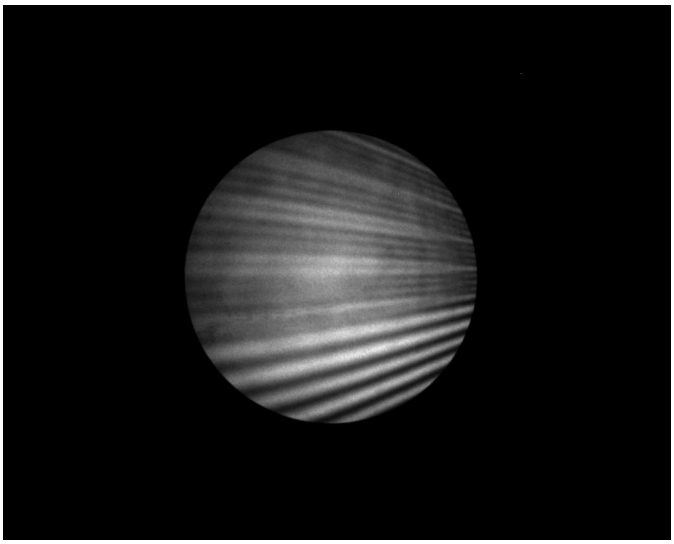

Figure 4.1: Image of eight lines per millimeter (above) and four lines per millimeter (below). Both lines can be seen. The viewing field is reduced to about 50%.

Mean diameter	$20\,\mu m$
Size distribution	$5 - 35\,\mu m$
Particle shape	non-spherical but round
Density	$1.03\,g/m^3$
Melting point	$175°C$
Refractive index	1.5
Material	polyamide 12

Table 4.1: Main characteristics of the particles used for preliminary measurements.

Our first PIV images

Preliminary tests have been carried out to check all the experimental setup. For such tests seeding particles without fluorescent dye are used to save costs. Dantec Dynamics' polyamide particles (see Table 4.1 for their main characteristics) have been employed. In fact these cheaper particles have a size distribution from $5\,\mu m$ to $35\,\mu m$, a range which turns out to be comparable to the lowest detectable value by our instruments.
In a first test we use water in a simple bid. The aim is simply to verify the goodness of the measurement chain (in particular of the software and the intensifier–camera system) and take some photos to correlate. The Dantec Dynamics' polyamide particles are used as tracers. Cross-correlation implemented in Matlab is used to estimate the particle veocity. The PIV analysis program (developed on purpose) correlates $32 \times 32\,pixel$ interrogation windows with a single-pass elaboration method. The interframing time is set at $6\,ms$, very close to the expected interframing time required in the real experiment to oserve the helical coil secondary flows. This test produces pairs of images as in Figure 4.2(a); cross-correlations of the two pictures produces the velocity field (Figure 4.2(b)). As can be seen, while the extension tube between camera and intensifier unit is not employed, half of the viewing field is lost.

4.2 Acknowledgments

Many people have helped us in the difficult and time-consuming process of starting the project up. What follows is only a partial list. Prof. Sergio DePonte is thanked for continuous help and suggestions. Prof. Carlo Osnaghi has helped us in the choice of the pump. Donato and Valentina have been a day-to-day helpful presence in the Aerodynamics lab, supervisioned by Gabriele Campanardi. The contributions by the coordinator of the workshop, Silvio Ferragina, together with Roberto Bertè (manufacturing and cylinder welding), Paolo Rubini (high-precision plate welding), Mauro Strada (manufacturing), Antonio Ravenna (steel cylinder and iron plate painting) are gratefully aknowledged. Last, this project has involved a number of suppliers and thus produced a sizeable amount of work for the administrative staff: their support is acknowledged.

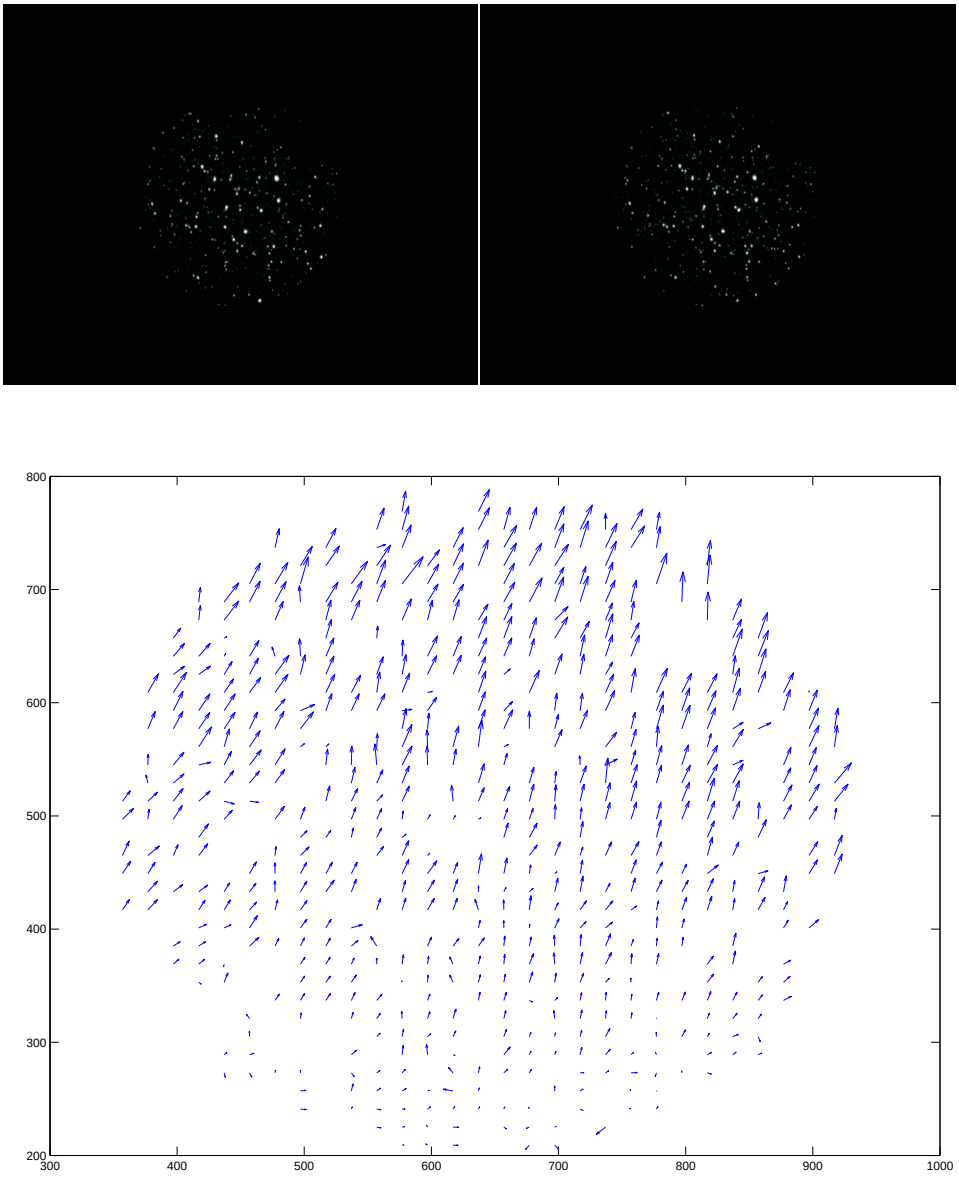

Figure 4.2: Preliminary test: (a) couple of the images of polyamide particles; (b) the velocity field obtained by cross-correlation.

Bibliography

[1] S. A. Berger, L. Talbot, L. S. Yao. Flow in curved pipes. *Annual Review of Fluid Mechanics*, 15:461–512, 1983.

[2] M. Vasudevaiah, R. Patturaj. Effecs of torsion in a helical pipe flow. *Internat. J. Math. and Math. Sci.*, 17(3):553–560, 1994.

[3] L. Zabielski, A. J. Mestel. Steady flow in a helically symmetric pipe. *Journal of Fluid Mechanics*, 370:297–320, 1998.

[4] T. J. Hüttl, C. Wagner, R. Friedrich. Navier–Stokes solutions of laminar flows based on orthogonal helical coordinates. *Int. J. Numer. Meth. Fluids*, 29:749–763, 1999.

[5] D. R. Webster, J. A. C. Humphrey. Experimental observations of flow instability in a helical coil. *Transaction of the ASME*, 115:436–443, 1993.

[6] D. R. Webster, J. A. C. Humphrey. Traveling wave instability in helical coil flow. *Physics of Fluids*, 9(2):407–418, 1997.

[7] C. X. Lin, M. A. Ebadian. The effects of inlet turbulence on the development of fluid flow and heat transfer in a helically coiled pipe. *International Journal of Heat and Mass Transfer*, 42:739–751, 1999.

[8] Y. Fan, R. I. Tanner, N. Phan-Thien. Fully developed viscous and viscoelastic flows in curved pipes. *Journal of Fluid Mechanics*, 440:327–357, 2001.

[9] T. J. Hüttl, R. Friedrich. Direct numerical simulation of turbulent flows in curved and helically coiled pipes. *Computers and Fluids*, 30:591–605, 2001.

[10] P. M. Ligrani, R. D. Niver. Flow visualization of Dean vortices in a curved channel with 40 to 1 aspect ratio. *Phys. Fluids*, 31(12):3605–3617, 1988.

[11] G. Belfort, H. Mallubhotla, W. A. Edelstein, T. A. Early. Bifurcation and application of Dean vortex flows. Evanston (IL), USA, 6-8 September 2001. 12th International Couette–Taylor Workshop.

[12] F. Schönfeld, S. Hardt. Simulation of helical flows in microchannels. *AIChE Journal*, 50(4):771–778, 2004.

[13] K. Yamamoto, X. Wu, K. Nozaki, Y. Hayamizu. Visualization of Taylor–Dean flow in a curved duct of square cross-section. *Fluid Dynamics Research*, 38:1–18, 2006.

[14] M. Raffel, C. E. Willert, J. Kompenhans. *Particle image velocimetry: a practical guide*. Springer, 1998.

[15] M. Germano. The Dean equations extended to a helical pipe flow. *Journal of Fluid Mechanics*, 203:289–305, 1989.

[16] A. Y. Gelfgat, A. L. Yarin, P. Z. Bar-Yoseph. Dean vortices-induced enhancement of mass transfer through an interface separating two immiscible liquids. *Physics of Fluids*, 15(2):330–347, 2003.

[17] Esdu. `www.esdu.com`.

[18] M. Quadrio, S. Sibilla. Numerical simulation of turbulent flow in a pipe oscillating around its axis. *Journal of Fluid Mechanics*, 424:217–241, 2000.

[19] S. Nakagawa, T. J. Hanratty. Particle image velocimetry measurements of flow over a wavy wall. *Physics of Fluids*, 13(11):3504–3507, 2001.

[20] tecnoCURVE. `www.tecnocurve.com`, San Pietro di Morubio (VR), Italy.

[21] Central Fabricators, Inc. `www.centralfabricators.com`, Cincinnati, Ohio, U.S.A.

[22] Marks Brothers, Inc. `www.marks-brothers.com`, Portland, Oregon, U.S.A.

[23] Roben Manufacturing, Inc. `www.robenmfg.com`, Lakewood, New Jersey, U.S.A.

[24] Tube & Coil Productions, Inc. `www.jfdcoil.com`, Hamden, Connecticut, U.S.A.

[25] Giacomo Abbadini & C. SAS. `www.abbadini.it`, Milan, Italy.

[26] I. E. Idelchik. *Handbook of hydraulic resistance*. Hemisphere publishing corporation, 1986.

[27] PCO. `www.pco.de`, Kelheim, Germany.

[28] Omega Optical, Inc. `www.omegafilters.com`, Brattleboro, Vermont, U.S.A.

[29] C. M. Zettner, M. Yoda. Particle velocity field measurements in a near-wall flow using evanescent wave illumination. *Experiments in Fluids*, 34:115–121, 2003.

[30] Distrilab BV. `www.distrilab.nl`, Leusden, Holland.

[31] Oxford Lasers. `www.oxfordlasers.com`, Didcot, Oxon, United Kingdom.

[32] Hamamatsu Photonics. `www.hamamatsu.com`, Hamamatsu City, Japan.

[33] CSF INOX S.p.A. `www.csf.it`, Montecchio Emilia (RE), Italy.

[34] TRE–I Fibre Ottiche. `www.tre-i.it`, Zanica (BG), Italy.

[35] FluxOptica S.r.l. `www.fluxoptica.com`, Milan, Italy.

[36] Dantec Dynamics A/S. `www.dantecdynamics.com`, Skovlunde, Denmark.

[37] SICURIT Alarmitalia S.p.A. `www.sicurit.net`, Milan, Italy.

[38] M.M. Montanari Massimo S.r.l. `www.mmtubi.com`, Conselice (RA), Italy.

[39] Italfer Folzini S.a.s. Via della Repubblica 45, 20030 Seveso (MI), Italy. Phone: 0362503382.

[40] Migliari Alluminio S.r.l. `www.migliarialluminio.it`, Settimo Milanese (MI), Italy.

[41] Fonderia Fazzini S.r.l. `www.fonderiafazzini.it`, Cardano al Campo (VA), Italy.

[42] La Politecnica S.r.l. `www.lapolitecnica.it`, Milan, Italy.

[43] UTP S.r.l. `www.utpsrl.it`, Dalmine (BG), Italy.